Spatial distribution of relaxation behavior on the surface of a ferroelectric relaxor in the ergodic phase

S. V. Kalinin,[1,a)] B. J. Rodriguez,[2] S. Jesse,[1] A. N. Morozovska,[3] A. A. Bokov,[4] and Z.-G. Ye[4]
[1]*Oak Ridge National Laboratory, Oak Ridge, Tennessee 37831, USA*
[2]*University College Dublin, Belfield, Dublin 4, Ireland*
[3]*V. Lashkaryov Institute of Semiconductor Physics, National Academy of Science of Ukraine, 41, Prospect, Nauki, 03028 Kiev, Ukraine*
[4]*Department of Chemistry and 4D LABS, Simon Fraser University, Burnaby, British Columbia V5A 1A6, Canada*

(Received 9 July 2009; accepted 11 September 2009; published online 5 October 2009)

Spatial homogeneity of polarization relaxation behavior on the surface of $0.9Pb(Mg_{1/3}Nb_{2/3})O_3-0.1PbTiO_3$ crystals in the ergodic relaxor phase is studied using three-dimensional time-resolved spectroscopic piezoresponse force microscopy. The number of statistically independent components in the spectroscopic image is determined using principal component analysis. In the studied measurement time interval, the spectra generally exhibit logarithmic behavior with spatially varying slope and offset, and the statistical distribution of these parameters are studied. The data illustrate the presence of mesoscopic heterogeneity in the dynamics of the relaxation behavior that can be interpreted as spatial variation in local Vogel–Fulcher temperatures. © *2009 American Institute of Physics*. [doi:10.1063/1.3242011]

Unique dielectric and electromechanical properties of relaxor ferroelectrics have attracted broad attention to the polarization switching and relaxation mechanisms in these materials.[1] Macroscopic techniques such as dielectric spectroscopy[2,3] and light scattering[4,5] unambiguously indicate the broad distribution of relaxation times,[3,6] related to the interactions and dynamics of polar nanoregions (PNRs). The link between the PNRs and the unusual properties of relaxors has stimulated a number of spatially resolved studies using piezoresponse force microscopy (PFM).[7–10] Even though the spatial resolution is significantly larger than the estimated size of a PNR (2–10 nm), these studies have provided insights into the relationship between disorder and *static* mesoscopic (~100 nm) polar structure. At the same time, little is known about the mesoscopic *dynamics* behavior. Here, we analyze the spatial variability of polarization relaxation in an ergodic ferroelectric relaxor using spatially resolved piezoresponse spectroscopy.[11]

The $(1-x)Pb(Mg_{1/3}Nb_{2/3})O_3-xPbTiO_3$ crystal with $x=0.1$ (PMN-10PT) is grown using a flux method.[12] The dielectric maximum occurs at $T_{max}=310$ K (at 1 kHz) and the crystal undergoes a macroscopically cubic to rhombohedral ferroelectric phase transition on cooling at $T_c \cong 280$ K (as determined by x-ray diffraction measurements).[13] The transition is observed only near the surface of the crystal while the bulk structure remains nearly cubic (as determined by neutron diffraction measurements).[14] The Burns temperature is ~650 K and the Vogel–Fulcher temperature is ~270 K. The absence of macroscopic piezoelectric effects[15] and aging[16] at $T>T_C$ suggests that the bulk room-temperature state in PMN-10PT is ergodic. The PFM measurements are performed using a commercial atomic force microscope (AFM) (Veeco MultiMode with Nanonis controller) on the mirror-polished and annealed (500 °C for 30 min) (100) surface. The spatially resolved relaxation measurements are performed using a homebuilt MATLAB/LABVIEW data acquisition system, as described elsewhere.[11]

The surface topography and domain structure before and after the switching experiment are shown in Fig. 1. The PFM amplitude and phase images indicate that a labyrinthine domain structure is ubiquitously present on the surface. The presence of these domain patterns indicates the deviation of symmetry from cubic to transversally isotropic. The presence of switchable polarization is clearly established from the contrast change after the switching experiment [Figs. 1(d)–1(f)]. Note that the switched contrast is significantly larger than the pre-existing domain contrast.

To probe polarization relaxation *locally*, dc bias pulses of specified magnitude and duration are applied to the conducting AFM tip in contact with the sample, and the resulting vertical electromechanical response is measured as a func-

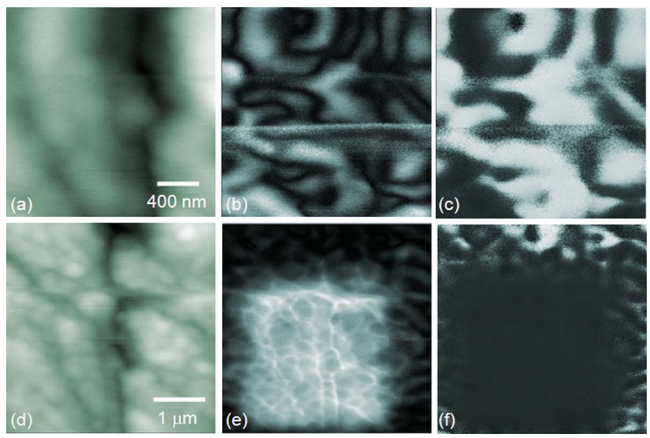

FIG. 1. (Color online) [(a) and (d)] Surface topography and piezoresponse [(b) and (e)] amplitude and [(c) and (f)] phase images before [(a), (b), and (c)] and after [(d), (e), and (f)] switching.

a)Author to whom correspondence should be addressed. Electronic mail: sergei2@ornl.gov.

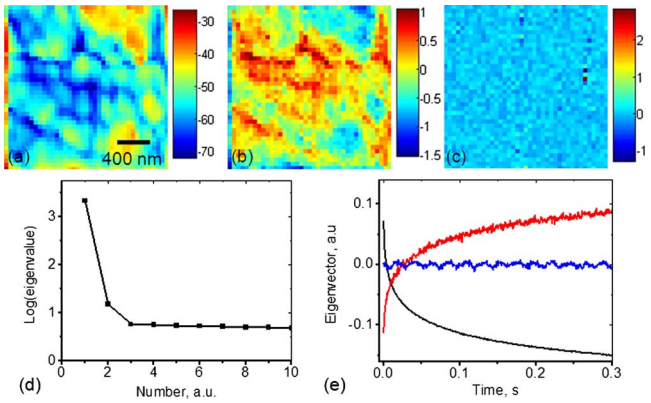

FIG. 2. (Color online) PCA decomposition of the time-resolved spectroscopic imaging data. [(a)–(c)] The principal component images $a_k(x,y)$ for $k=1..3$ (2×2 μm^2). (d) The eigenvalue (scree) plot and (e) the first three eigenvectors, $w_j(t_j)$.

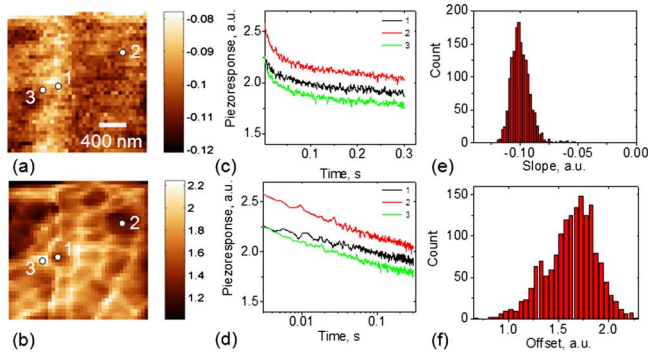

FIG. 3. (Color online) Spatially resolved maps of (a) slope, B_1 and (b) offset, B_0 of the logarithmic relaxation law (2×2 μm^2). Relaxation curves in selected locations in (c) linear and (d) logarithmic scale. Histograms of the (e) slope and (f) offset.

tion of time. The measurements are performed on a densely-spaced grid of points, yielding the three-dimensional (3D) $PR(x,y,t)$ data arrays, where PR is the piezoresponse signal, (x,y) is the coordinate, and t is time. Here, the measurements are performed with a 30 ms, 10 V setting pulse, and a 300 ms detection window (4000 time samples) on a 40×40 spatial grid with 50 nm pixel spacing.

Analysis of the resulting $PR(x,y,t)$ using the functional fit, $PR(t)=f(\alpha,t)$, where $\alpha=\alpha_1,..,\alpha_n$ is an n-dimensional parameter vector, allows maps of $\alpha_i(x,y)$ describing the spatial variability of the relaxation behavior to be constructed. As an example, a fit using the stretched exponential law, $PR(t)=A_0+A_1\exp[-(t/\tau)^\beta]$ with $n=4$ yields spatially resolved maps of relaxing, A_1, and nonrelaxing, A_0, polarization components, relaxation time, τ, and exponent, β.[17] However, such analysis is prone to errors, since the functional form of the relaxation law, its physical interpretation, and the number of statistically independent variables are *a priori* unknown. As a result, fitting can lead to a strong interdependence of the derived parameters, α, yielding poorly interpretable maps.

To avoid this problem and to establish unambiguously the veracity of the fitting procedure, we analyze spectroscopic PFM data using principal component analysis (PCA).[18–20] The spectroscopic image of $N\times M$ pixels formed by spectra containing P points is represented as a superposition of the eigenvectors w_j,

$$PR_i(t_j)=a_{ik}w_k(t_j), \tag{1}$$

where $a_{ik}\equiv a_k(x,y)$ are position-dependent expansion coefficients, $PR_i(t_j)\equiv PR(x,y,t_j)$ is the image at a selected time, and t_j are the discrete times at which the response is measured. The eigenvectors, $w_k(t)$, and the corresponding eigenvalues, λ_k, are found from the covariance matrix, $\mathbf{C}=\mathbf{A}\mathbf{A}^T$, where $\mathbf{A}$ is the matrix of all experimental data points $\mathbf{A}_{ij}=PR_i(t_j)$, i.e., the rows of $\mathbf{A}$ correspond to individual grid points $(i=1,..,N\cdot M)$, and the columns correspond to time points, $j=1,..,P$. The eigenvectors, $w_k(t_j)$, are orthogonal and are chosen such that the corresponding eigenvalues are placed in descending order, $\lambda_1>\lambda_2>....$

The spatial maps of the first three PCA components of the piezoresponse data arrays and the corresponding eigenvectors and eigenvalues are shown in Fig. 2. The shape of $\lambda_k(k)$ dependence (scree plot) indicates that the first two PCA components contain 99.9% of the significant information within the 3D spectral image, whereas the remaining $P-2=3998$ components are dominated by noise. This behavior is also evident from the eigenvectors, $w_i(t_j)$, where first two eigenvectors illustrate a clear time dependence, while the third and subsequent eigenvectors are noiselike. Finally, spatially resolved maps of the first and second PCA components clearly illustrate long-range contrast and discernible spatial features, whereas the third and subsequent PCA maps are essentially random.

This analysis suggests that with the given experimental noise limit and measurement time interval, the 3D spectroscopic relaxation image can be represented as a system with 2 degrees of freedom, $PR(x,y,t)=a_1(x,y)w_1(t)+a_2(x,y)w_2(t)+Y(t)$, where $Y(t)$ is a spatially uncorrelated noise term. Therefore, functional fits with more than two independent parameters will invariably lead to strong parameter dependence, and provide unrealistic results. Note that the PCA analysis is a purely statistical method and does not employ any assumption regarding the underlying physical behavior, ensuring its fidelity.

The detailed analysis of the eigenvectors and single-point relaxation data suggest that the observed behavior is close to logarithmic, $PR(t)=B_0+B_1\ln t$. Given the results of the PCA analysis, the use of more complex functional fits is not expected to provide better description of the data. Hence, 3D $PR(x,y,t)$ data arrays were fitted using a logarithmic function and the resulting spatial maps of offset, $B_0(x,y)$, and slope, $B_1(x,y)$, are shown in Figs. 3(a) and 3(b). Note that both maps indicate the presence of mesoscopic structures and contain a number of uncorrelated features, indicative of the validity of the analysis.

A number of relaxation curves extracted from regions of dissimilar contrast in Figs. 3(a) and 3(b) are shown in Figs. 3(c) and 3(d). Note that the relaxation behavior varies between adjacent locations, illustrating the presence of mesoscopic dynamic inhomogeneity on the surface of the PMN-10PT relaxor crystal. The histograms of the slope and offset are shown in Figs. 3(e) and 3(f). The slope distribution is relatively narrow, $B_1=-0.10\pm0.02$ within the image, and close to Gaussian. In comparison, the distribution of offsets is much broader, $B_0=1.5\pm0.5$, and is strongly asymmetric. The observed point-to-point variations in the amplitude of the pulse-induced polarization can be attributed to a variation

of PNR density, the presence of lattice defects and surface contamination (the latter factor is probably responsible for the distribution asymmetry), and (possibly) topographic cross-talk, while the distribution of logarithmic slope suggests nonuniform relaxation kinetics.

To get insight into the origins of the observed mesoscopic dynamic heterogeneities, we consider standard relaxation dynamics, $dP/dt=-P/\tau$, equivalent to relaxation, $P=P_0\exp(-t/\tau)$. To relate the materials parameters to the relaxation law we assume that the local relaxation time is determined by the activation energy, E, and depends on temperature in accordance with the Vogel–Fulcher relationship, $\tau(E)=\tau_0\exp[E/(T-T_f)]$. Then, in terms of a distribution function of energies, $G(E)$, the relaxation law is expressed as

$$\langle P\rangle = P_0\int_{E_{\min}}^{E_{\max}} dEG(E)\exp\left[-\frac{t}{\tau(E)}\right]. \tag{2}$$

Equation (2) leads to $G(E)\equiv(T-T_f)^{-1}\tau(E)g[\tau(E)]$. For systems with logarithmic relaxation the energy distribution is almost uniform, $G(E)\approx(E_{\max}-E_{\min})^{-1}$ and Eq. (2) can be integrated in the analytical form. For $\tau_{\min}\ll t\ll\tau_{\max}$, where $\tau_{\min,\max}=\tau_0\exp[E_{\min,\max}/(T-T_f)]$, we obtain

$$\langle P(t)\rangle \approx -P_0\left[\frac{T-T_f}{E_{\max}}\gamma-1+\frac{T-T_f}{E_{\max}}\ln\left(\frac{t}{\tau_0}\right)\right], \tag{3}$$

where the Euler constant $\gamma=0.577$. Hence, the spatial variation of slope in response-time dependence for the logarithmic model can be interpreted as the fluctuations of the local Vogel–Fulcher temperature. This interpretation is in agreement with the experimental observation of the distribution of the Vogel–Fulcher temperatures related to various segments of the dielectric relaxation spectrum in the relaxor crystal (higher values of T_f correspond to slower segments of the spectrum).[2] These segments can be related to various mesoscopic regions of the crystal.

To summarize, the spatial variability of relaxation behavior in the ergodic relaxor phase of a PMN-10PT crystal surface is studied using time-resolved piezoresponse spectroscopy. The principal component analysis of the 3D spectroscopic imaging data sets indicates that within the image (40×40 pixels, 2×2 μm^2), the spectra in the time domain (0.3 s, 4000 pixels) can be represented as a sum of two statistically independent components, imposing the limit on the number of independent parameters that can be determined in a functional fit. The two-parameter logarithmic fit allows a nearly-ideal description of experimental relaxation behavior within the image. Spatially resolved maps of logarithmic function slope and offset illustrate the presence of mesoscopic dynamic heterogeneities on the surface of the relaxor crystal. These heterogeneities can be interpreted as spatial variations of the Vogel–Fulcher temperature.

The research is supported by the Center for Nanoscale Materials Sciences (S.V.K., B.J.R., and S.J.) at the Oak Ridge National Laboratory, Division of Scientific User Facilities, Office of Basic Energy Sciences, U.S. Department of Energy and was a part of the CNMS User Program (Grant No. CNMS2007-085). This work is also supported (A.A.B. and Z.G.Y.) by the Office of Naval Research (Grant No. N00014-06-1-0166). B.J.R. also acknowledges the support of UCD Research.

[1] W. Kleemann, J. Mater. Sci. **41**, 129 (2006).
[2] A. Levstik, Z. Kutnjak, C. Filipic, and R. Pirc, Phys. Rev. B **57**, 11204 (1998).
[3] A. A. Bokov and Z. G. Ye, Phys. Rev. B **74**, 132102 (2006).
[4] J.-H. Ko, D. H. Kim, and S. Kojima, Phys. Rev. B **77**, 104110 (2008).
[5] J.-H. Ko, S. Kojima, A. A. Bokov, and Z.-G. Ye, Appl. Phys. Lett. **91**, 252909 (2007).
[6] W. Kleemann and R. Linder, Ferroelectrics **199**, 1 (1997).
[7] A. Gruverman and A. Kholkin, Rep. Prog. Phys. **69**, 2443 (2006).
[8] V. V. Shvartsman and A. L. Kholkin, Phys. Rev. B **69**, 014102 (2004).
[9] V. V. Shvartsman, A. L. Kholkin, A. Orlova, D. Kiselev, A. A. Bogomolov, and A. Sternberg Appl. Phys. Lett. **86**, 202907 (2005).
[10] V. V. Shvartsman and A. L. Kholkin, J. Appl. Phys. **101**, 064108 (2007).
[11] B. J. Rodriguez, S. Jesse, J. Kim, S. Ducharme, and S. V. Kalinin, Appl. Phys. Lett. **92**, 232903 (2008).
[12] M. Dong and Z.-G. Ye, J. Cryst. Growth **209**, 81 (2000).
[13] Z.-G. Ye, Y. Bing, J. Gao, A. A. Bokov, P. Stephens, B. Noheda, and G. Shirane, Phys. Rev. B **67**, 104104 (2003).
[14] P. M. Gehring, W. Chen, Z.-G. Ye, and G. Shirane, J. Phys.: Condens. Matter **16**, 7113 (2004).
[15] W. Y. Pan, W. Y. Gu, D. J. Taylor, and L. E. Cross, Jpn. J. Appl. Phys., Part 1 **28**, 653 (1989).
[16] D. Viehland, J. F. Li, S. J. Jang, L. E. Cross, and M. Wittig, Phys. Rev. B **43**, 8316 (1991).
[17] S. V. Kalinin, B. J. Rodriguez, J. D. Budai, S. Jesse, A. N. Morozovska, A. A. Bokov, and Z.-G. Ye, arXiv: 0808.3827v1.
[18] S. Jesse and S. V. Kalinin, Nanotechnology **20**, 085714 (2009).
[19] N. Bonnet, Micron **35**, 635 (2004).
[20] M. Bosman, M. Watanabe, D. T. L. Alexander, and V. J. Keast, Ultramicroscopy **106**, 1024 (2006).